LBL-38460
UC-400

Lawrence Berkeley Laboratory

UNIVERSITY OF CALIFORNIA

ENERGY & ENVIRONMENT DIVISION

Presented at the Spring 1996 Meeting of the Western States Section of the Combustion Institute, Tempe, AZ, March 11–12, 1996, and to be published in the Proceedings

PLIF Investigation of the Evolution of Premixed Turbulent Flame Structures

B. Bédat, I.G. Shepherd, and R.K. Cheng

March 1996

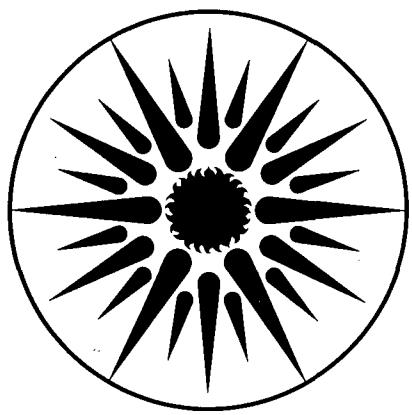

ENERGY AND ENVIRONMENT DIVISION

Prepared for the U.S. Department of Energy under Contract Number DE-AC03-76SF00098

DISCLAIMER

LBL 38460
UC-400

PLIF Investigation of the Evolution of Premixed Turbulent Flame Structures

B. Bédat, I. G. Shepherd and R. K. Cheng

Energy & Environment Division
Ernest Orlando Lawrence Berkeley National Laboratory
University of California
Berkeley, CA

March 1996

This work was supported by the Director, Office of Energy Research, Office of Basic Energy Sciences, Chemical Sciences Division of the U.S. Department of Energy under Contract No, DE-AC03-76SF00098

PLIF Investigation of the Evolution of Premixed Turbulent Flame Structures

B. Bédat, I. G. Shepherd and R. K. Cheng

Combustion Group
Ernest Orlando Lawrence Berkeley National Laboratory
Berkeley, CA

Abstract

Planar Laser Induced Fluorescence (PLIF) technique of OH has been used to investigate premixed turbulent flame structures under moderate and intense isotropic turbulence. The goal is to test and verify theoretical assumptions regarding classification of premixed turbulent flames. The experiments use a weak-swirl burner that supports stable combustion in laminar and turbulent flames with incident turbulence intensities exceeding 20%. OH-PLIF results obtained for a flame with Ka = 0.8 (i.e. corrugated flamelet regime) show that the flame forms deep flame cusps but not flame pockets. For a flame with Ka = 3.1 (i.e. distributed reaction zone regime), the flame front is more fragmented with pockets form both in the products and in the reactants. Sharp rises in the OH fluorescence intensity profiles deduced from both flames suggest flamelet behavior even for conditions well within the regime of "distributed reaction zones".

Introduction

The concept of classifying premixed turbulent flames into different regimes evolved from the idea of Damköhler [1]. It remains an important guiding principle for both experimental and theoretical works. Various criteria to differentiate the regimes of premixed turbulent flames have been postulated. These regimes are usually expressed on phase diagrams as functions of non-dimensional quantities derived from the mixture properties, and time and length scales of the incident turbulence [2-4]. These non-dimensional quantities are the turbulent Reynolds number, Re_t, the Damköhler number, Da and the Karlovitz number, Ka. Figure 1 shows Borghi's version which is also known as the Borghi-Barrère diagram. The underlying assumption of this and all other similar phase diagrams is that the scaling laws for non-shear isotropic turbulence are required to relate Da and Ka to Re. Accordingly, $Da = (l_t/d_L)\,(u'/S_L)^{-1}$ and $Ka = (u'/S_L)^{3/2}\,(l_t/d_L)^{-1/2} = (d_L/l_k)^2$ [4]. The reaction zone thickness, d_L is defined by the original Klimov criterion $d_L\,S_L = \nu$. The Ka = 1 boundary, generally known as the Klimov-Williams criterion, separates the regimes of wrinkled laminar flames that have thin reaction zones from flames with thicker distributed reaction zones.

Due to the difficulties in generating intense isotropic turbulence, previous experimental investigations [5, 6] have used shear turbulence to achieve the necessary high turbulence

intensities and have applied (though unintentionally) the non-shear turbulence scaling laws to shear turbulence. In a recent paper [7], we reported the development of a burner for stabilizing premixed turbulent flames in intense isotropic turbulence of up to 20%. This burner offers an experimental configuration that satisfies all the turbulence scaling law as prescribed by the Borghi-Barrère diagram. Our burner has two special features. It has a turbulence generator adapted from a design originated by Videto and Santavicca [8] and uses weak-swirl generated by air jets [9,10] for stabilizing flames in the intense isotropic turbulent flows. This set-up produces stable premixed turbulent flames under a wide range of mixture conditions and turbulence intensities. The four experimental conditions [7] (Table 1) were designed to investigate systematically the flame on both sides of the Klimov-Williams criterion, i.e. Ka = 1.

In our previous study, laser Doppler anemometry and Rayleigh scattering techniques were the diagnostics. The velocity statistics show that flames in intense turbulence (Cases III and IV, Ka > 1) have little effect on the velocity statistics. The probability density functions (pdf) deduced from Rayleigh scattering measurements are clearly bi-modal and show very little differences between flames with moderate (Case II) and intense turbulence (Case IV). These results support recent theoretical analyses [11, 12] that the flamelets are perhaps more resilient to penetration of small eddies than predicted by the Klimov-Williams criterion. The point measurements, however, cannot fully validate our preliminary conclusions. The use of more sophisticated 2-D techniques are required.

To obtain a better understanding of the evolution in flame structures with increasing Ka to above 1, the present study uses the PLIF (Planar Laser Induced Fluorescence) technique for OH radicals. OH is a convenient marker of the reaction zone because its concentration increases sharply at the leading edge (i.e. facing the cold reactants) of the flame. Once generated, OH radicals are removed by relatively slow third-body recombination reactions and decay slowly in the products away from the reaction zone. OH radicals produce a strong fluorescence signal that facilitates optimizing the signal to noise ratio. Though the calibration of the PLIF system to obtain quantitative measurement of 2D OH concentrations is laborious and remains a subject of ongoing research, our PLIF system is sufficiently sensitive to quantify gross changes in local flame thickness, and is also suitable for characterizing local flame wrinkle geometry, flame lift-off and local quenching.

Experimental Set-up

The schematic of the weak-swirl burner is shown in Fig 2. It has a settling chamber, a turbulence generator which incorporates a converging nozzle, and a 50 mm diameter, 233 mm long tube section where the swirler is attached. The turbulence generator is an adaptation of the linear slot design of Videto and Santavicca [8] to circular geometry. It has a 0.8 mm wide 107 mm diameter axisymmetric slot. Premixed CH_4/air flow passes through this slot and impacts with a converging nozzle (contraction ratio = 7) which breaks down the large vortical structures generated downstream of the slot. The swirl generator is placed 130 mm above the converging nozzle. It consists of four 2.5 mm diameter , individually adjustable, tangential air jets inclined at 20°. The swirl rate is

monitored by a rotometer which measures the total injection air flow. A 103 mm extension placed above the swirler allows the swirl to developed. The exit rim of the burner is tapered at 45° to prevent the formation of a recirculation zone above the rim. The swirl number, S, given by Claypole and Syred [13] applies to this burner and the previous version [9,10]. Table I shows the four experimental conditions and relevant turbulence scales.

Diagnostic

In addition to PLIF, we also used tomography as a complimentary technique . The tomographic system has a sufficiently large field-of-view to capture the entire turbulent flame zone. PLIF has a smaller field-of-view and it is better suited for showing finer details of the reaction zones. Tomography is a simple diagnostic that requires seeding the premixed reactants with a silicone oil aerosol that burns and evaporates at the flame front. When illuminated with a laser sheet, the flame boundary separating the hot products from the cold reactant is delineated. The tomography and PLIF systems share a Spectra-Physics Quanta-ray DCR-2A Nd:YAG laser. This laser has a pulse energy of 400 mJ/pulse (@ 532 nm) with a pulse width of 8 nsec. For tomography The laser beam is formed into a sheet of 75 mm height and about 200 μm thick. Changing the sheet height is possible by varying the placement of the cylindrical lenses. The camera captures a field-of-view up to 120 mm x 120 mm.

For PLIF the second harmonics of the Nd:Yag laser pumps a Spectra Physics Quanta Ray dye laser that uses Rhodamine 590 dye. A frequency doubling crystal for the dye laser output generates a ultra-violet (UV) beam that is tuned to the $P_1(2)$ absorption transition (282.58 nm) of OH (1,0) band of the $A^2\,\Sigma^+ \leftarrow X^2\,\Pi$ system. OH fluorescence at 306.4 nm is detected by the use of narrow band filters placed in front of an intensified Xybion CCD camera. This system is capable of producing tunable output up to 50 mJ/pulse. For PLIF, the laser beam is shaped into a thin (less than 200 nm) vertical sheet of 30 mm in height to obtain sufficiently high light density to optimize the signal to noise ratio. The PLIF system has a field-of-view of 40 mm by 40 mm. This is sufficient to capture the largest relevant flame wrinkles and to span across most turbulent flame brush.

The tomography and PLIF systems share many common electronic components and data acquisition software. The laser pulse rate of 10 Hz provides the synchronization signal for the CCD camera and a six-buffer video board. The data acquisition software has the option to record and store the images continuously for post-processing. For this study, we have obtained 24 frames for each experiments. Since our PLIF system has yet to be calibrated for measuring quantitative concentrations, we have taken great care to ensure that all the experiments were performed with the same laser power and settings of the intensify camera. To provide baseline cases for comparison, PLIF images of laminar v-flames and conical flames were also obtained. OH fluorescence intensity profiles through the laminar flame are useful to infer the changes in flame front structures in turbulent flames.

Results

The experimental conditions investigated by tomography span the Klimov-Williams criterion (Ka = 1). The original weak-swirl burner with a co-flow of air [9,10] was used for the moderate turbulent flames with wrinkled flamelets, while the new burner was used for the high turbulence cases. Figure 3 compares two flames, SWF12 of Ref. [10] and Case IV. SWF12 is a stoichiometric methane/air flame with 7.5% turbulence generated by a perforated plate. It is well within the wrinkled flamelet regime. Case IV, as shown by its turbulence scales and intensities (Table 1), is considered to be within the "distributed reaction zone" regime. In tomography, the reactants appear bright due to the illumination of the oil aerosol by the laser sheet. Therefore, the tomographic records of Figure 3 also show the divergence of the reactants induced by weak-swirl. For SWF12, the co-flowing air prevents the formation of a shear layer at the edges (left and rights sides) of the reactant stream. The blurry boundary represent diffusion of the reactant into the co-flow air. The sharp boundary at the top is the wrinkled flamelet. These flame wrinkles are quite similar to those observed in flames stabilized by a stagnation plate [14]. The only differences seem to be that the wrinkles of SWF12 have deeper flames cusps and the wrinkles are uniform across the flame brush. This result is very encouraging because non-uniformity of the flame wrinkles may lead to uncertainties in the analyses of flame scales.

The burner for Case IV has no co-flow and the tomographic image shows that the mixing layer formed between the reactants and ambient air can have relatively large structures. These structures do not seem to have a significant effects on the flame. The difference between the flame wrinkles of SWF12 and Case IV is quite striking. The smooth large flame wrinkles of SWF12 are replaced by much more irregular and corrugated flame of Case IV. There is evidence that flame pockets are formed in the products as well as in the reactants. The flame brush thickness is also increase substantially. The thickening of the flame brush is in accord with our Rayleigh scattering measurements and show that the thick flame brush is not generated by flame bouncing. The tomography also shows some flame asymmetry (e.g. the Case IV flame as shown in Figure 3 is skewed to the left). This asymmetry tends to be random and is averaged-out in the mean. Therefore it is not observed by Rayleigh scattering. This is, however, important information for our PLIF investigation for it explains why the smaller PLIF field-of-view can occasionally miss the flame. The tomographic record of Case IV also demonstrates that this technique cannot resolve very fine flame wrinkles. The limitation is due to the aerosol seeding density. In the region near the top of the image, the flame boundary can be as diffused as the boundary between the reactants and the room air.

Shown in Figure 4 are two sets of OH-PLIF images for Cases II (flamelet regime) and IV (distributed reaction zone regime). As OH is formed at the flame front and persists in the products, this region appears bright. The boundary between the bright products and the dark reactants below is the flame front. The top edge of the laser sheet is also visible in these frames. Due to the three times difference in the fields of view, the scale for the OH-PLIF images as shown in Figure 4 is equal to that of the tomographic images of Figure 3.

For Case II (Figure 4(a)) with moderate turbulence, the flame is only slightly wrinkled and typical size of these wrinkles are comparable to the integral length scale of l_t = 15 mm. These wrinkles are not much different that those shown by the tomographic images of SWF12 (Figure 3) and those of stagnation point flames. The series of PLIF images also confirm that the degree of flame wrinkling varies greatly from one instance to another, for example, Frame 1 is much less wrinkled than Frame 5. The statistical nature has been reported in our earlier study of the fractal dimension of flame wrinkling and seem to suggest that the behavior is not confined to the stagnation flame configuration. Even at this condition close to Ka = 1 boundary, no flame pockets have been observed, the formation of deeper flame cusps seems to be the most noticeable change in flame front feature. Most of the flame fronts are oriented toward the reactants, with the exception of Frame 6. The change in flame front orientation towards the products is associated with the large flame cusps seen on the left of Frame 6.

The features of the flame wrinkles change drastically when turbulence intensity is increased (Figure 4(b)). At the higher turbulence level we have investigated (q'/S_L = 7.1) the flame front is more fragmented and forms pockets in both reactants and products.. Consequently, the flame front orientations with respect to the mean flow direction are much more random than in Case II. It is difficult, however, to establish if the flame pockets are detached. For example, the deep long flame front excursion into the products, shown near the center of Frame 1 suggests that a dissection perpendicular to the PLIF plane may show flame pockets similar to those of Frame 2. Also shown in Frames 1 and 5 are large portion of the flame fronts propagates into the downstream direction. The scales of flame wrinkles are clearly smaller. All these features indicate a large increase in the flame surface density [15] and a significant increase in the local burning rate.

To compare the flame fronts, Figure 5 shows OH fluorescence intensity profiles extracted from two frames (Frame 5 of Case II and Frame 5 of Case IV). From these profiles it would be possible to obtain further information to show if any significant change occurs between the two cases (II, Ka = 0.8 and IV, Ka = 3.1). The path of the profiles of Case II is chosen at a position where the flame fronts are normal to its direction. The sharps transitions are the flame fronts and the steady decrease in OH-PLIF intensity from r = 20 to -20 is caused by laser absorption effects. The transitions at r = 0, 15 mm are sharp and comparable to normal laminar flames. The transition at r = -5 mm is less steep and can be explained by the slightly out of normal flame front orientation. This shows the apparent flame thickening that can be introduced by random orientations in the out-of-plan direction.

Similar features are observable for Case IV. There are both sharp transitions (at r = 18, 12, 3 and 0 mm) and apparent flame front broadening. From the PLIF image, it is clear that the broadening are caused by the out-of-plane effects. Therefore, the PLIF results do not seem to suggest a significant change in flame front structure for flames with Ka > 1. This lend further support to our earlier conclusion that premixed turbulent flames seem to be more resilient to the penetration of small intense vortices than predicted by some theories.

Conclusion

Tomography and Planar Laser Induced Fluorescence (PLIF) technique of OH have been used to investigate premixed turbulent flame structures under moderate to very intense isotropic turbulence. The goal is to test and verify theoretical assumptions regarding the differences between flames classified as wrinkled laminar flame (under moderate turbulence), corrugated flames and flames with distributed reaction zones (under intense turbulence). The experiments use a weak-swirl burner that supports stable combustion in laminar and turbulent flames with incident turbulence intensities that exceeds 20%.

The large field-of-view afforded by tomography is useful for observing the overall behavior of the flame brush and helps the interpretation of PLIF observations (will 1/3 the field-of-view) within the context of the larger overall flame features. OH-PLIF results obtained for a flame with Ka = 0.8 (i.e. corrugated flamelet regime) show that the flame forms deep flame cusps but not flame pockets. The flame wrinkle scales remain comparable to the integral length scale of 15 mm. For a flame with Ka = 3.1 (i.e. distributed reaction zone regime), the flame front is more fragmented with pockets form both in the products and in the reactants. OH fluorescence intensity profiles were used to infer the changes in flame front structures. Sharp transitions on the profile shown by both flames suggest flamelet characteristics even for conditions well within the regime of "distributed reaction zones".

Acknowledgment

This work was supported by the Director, Office of Energy Research, Office of Basic Energy Sciences, Chemical Sciences Division of the U. S. Department of Energy under Contract No. DE-AC03-76SF00098. The authors would like to acknowledge Mr. Gary Hubbard for writing the computer controlled and data reduction software.

References

1. Damköhler, G., *Elektrochem.*, 46:601 (1940). English translation : The Effects of Turbulence on the Flame Velocity in Gas Mixtures. N.A.C.A. TM. p. 1112 (1947).
2. Bray, K. N. C., *Turbulent Reacting Flows*, Editors: P. A. Libby and F. A. Williams, Springer, Berlin, 1980, pp. 115.
3. Borghi, R. On the Structures and Morphology of Turbulent Premixed Flames, Recent Advances in the Aerospace Sciences. Editor : Forradi Casci, Plenum, 1985, pp. 117-138.
4. Peters, N., *21st Symposium (Int'l) on Combustion, The Combustion Institute*, Pittsburgh, 1986 pp. 1231-1250.
5. Bédat, B., and Cheng, R. K., *Combustion and Flame*, Vol. 100, 3, pp. 485-494 (1995).
6. Furukawa, J., Harada, E., and Hirano, T., *23rd Symposium (Int'l) on Combustion*, The Combustion Institute, Pittsburgh, 1992, pp. 789-794.

7. Yoshida, A., Narisawa, M., and Tsuji, H., *24th Symposium (Int'l) on Combustion*, The Combustion Institute, Pittsburgh, 1992, pp. 519-525.

8. Videto, B. D., and Santavicca, D. A. *Combustion Science and Technology*, 76:159-164 (1991).

9. Chan, C. K., Lau, K. S., Chin, W. K., and Cheng R. K., *24th Symposium (Int'l) on Combustion*, The Combustion Institute, Pittsburgh, 1992, pp. 511-518.

10. Cheng, R. K., *Combustion and Flame*, Vol. 101, pp. 1-14 (1995).

11. Poinsot, T., Veynante, D. and Candel, S., *23rd (Int'l) Symposium on Combustion*, The Combustion Institute, Pittsburgh, 1990 pp. 613-619

12. Jarosinski, J., Combustion and Flame, 56 : 337 (1984).

13. Claypole T. C. and Syred N. *18th Symposium (Int'l) on Combustion*, The Combustion Institute, 1981, p. 81.

14. Shepherd, I. G., Cheng, R. K., and Goix, P. J., *23rd (Int'l) Symposium on Combustion*, The Combustion Institute 1990, p. 781.

15. Bray, K.N.C., *Proc. Roy. Soc. A.,* Vol. 431, pp 313-335 (1990)

Table I Experimental Conditions and Relevant Parameters

Case	I	II	III	IV
Velocity [m/s]	2.00	3.00	5.00	7.00
S	-	0.09	0.08	0.06
u' [m/s] at c = 0.05	0.52	0.89	1.30	1.70
v' [m/s] at c=0.05	0.53	1.00	1.00	1.25
q' [m/s] at c= 0.05	0.37	0.67	0.82	1.06
l_t [mm]	15.00	15.00	15.00	15.00
Re_{l_t}	490	840	1220	1600
η (mm)	0.15	0.1	0.07	0.06
Φ	0.80	0.65	0.60	0.60
S_L[m]	0.30	0.18	0.15	0.15
d_L [mm]	0.05	0.08	0.1	0.1
q'/S_L	1.3	3.7	5.5	7.1
u'/S_L	1.8	5.0	8.8	11.5
Da	165.2	36.2	17.5	13.4
Ka	0.1	0.8	2.1	3.1
d_T [mm]	26.70	25.50	26.00	35.00

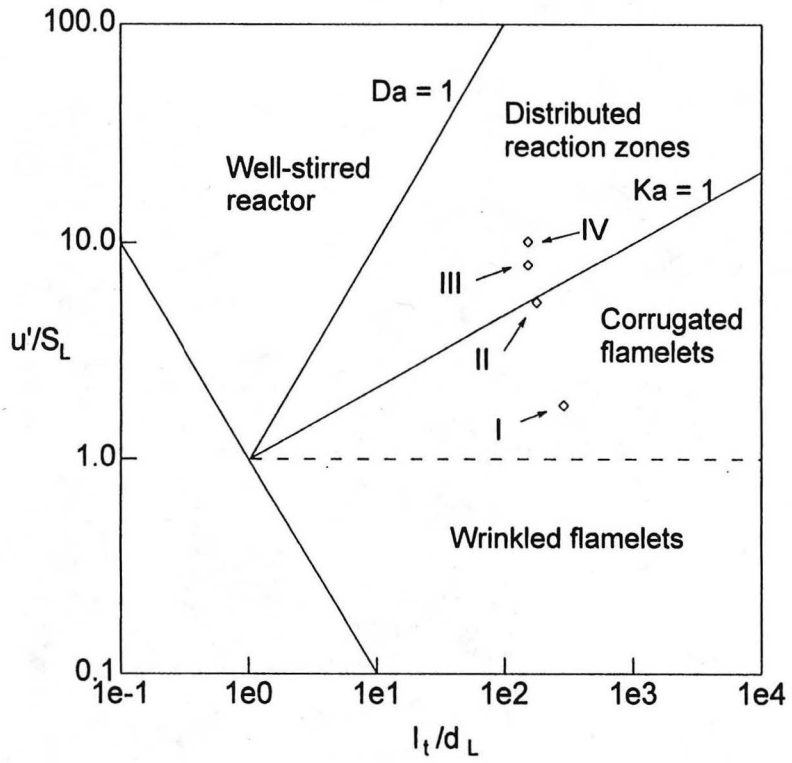

Figure 1 Regimes of premixed turbulent flames

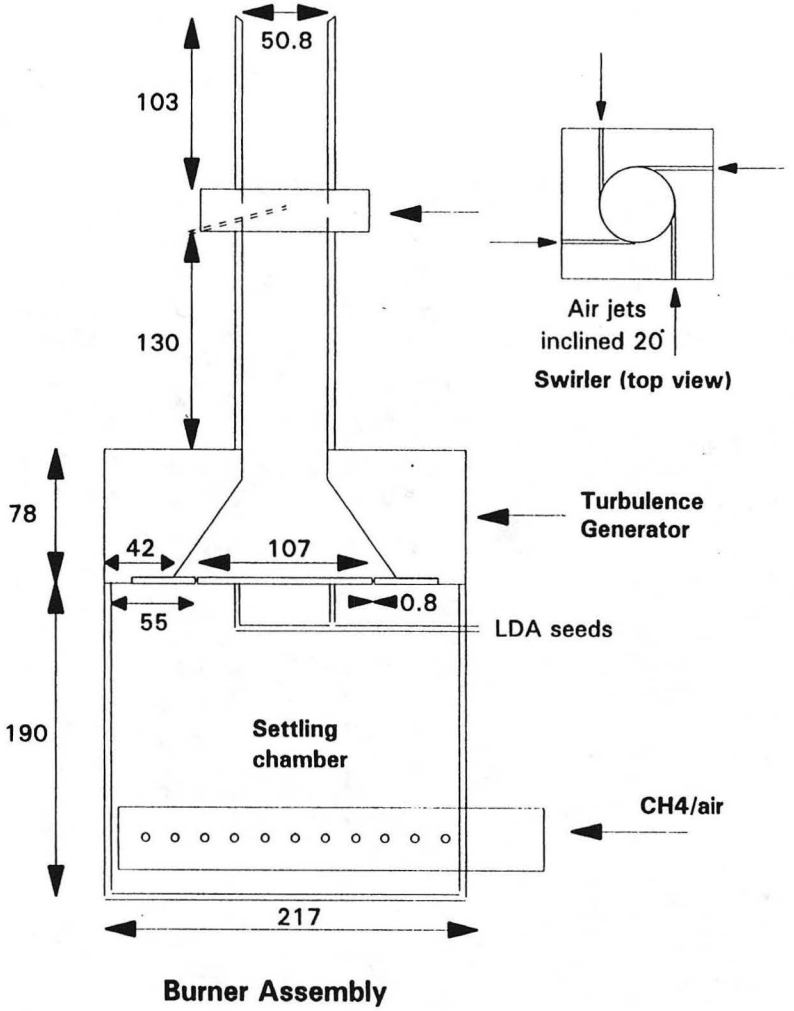

Figure 2 Schematic of the burner, all unites are in mm.

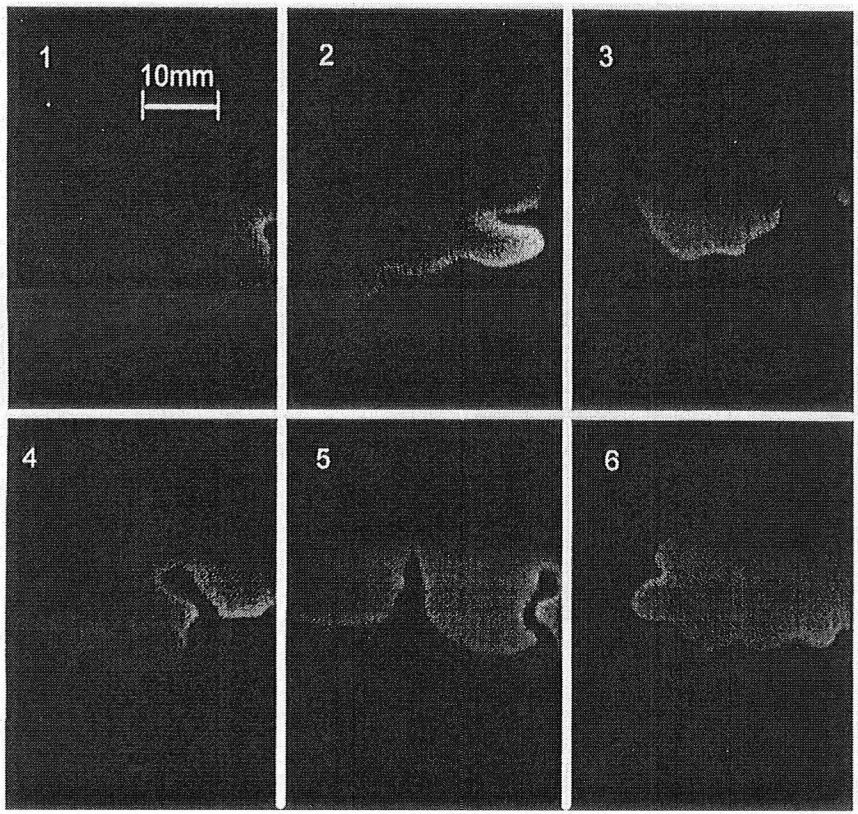

Figure 4 (a) OH-PLIF images of SWF12.

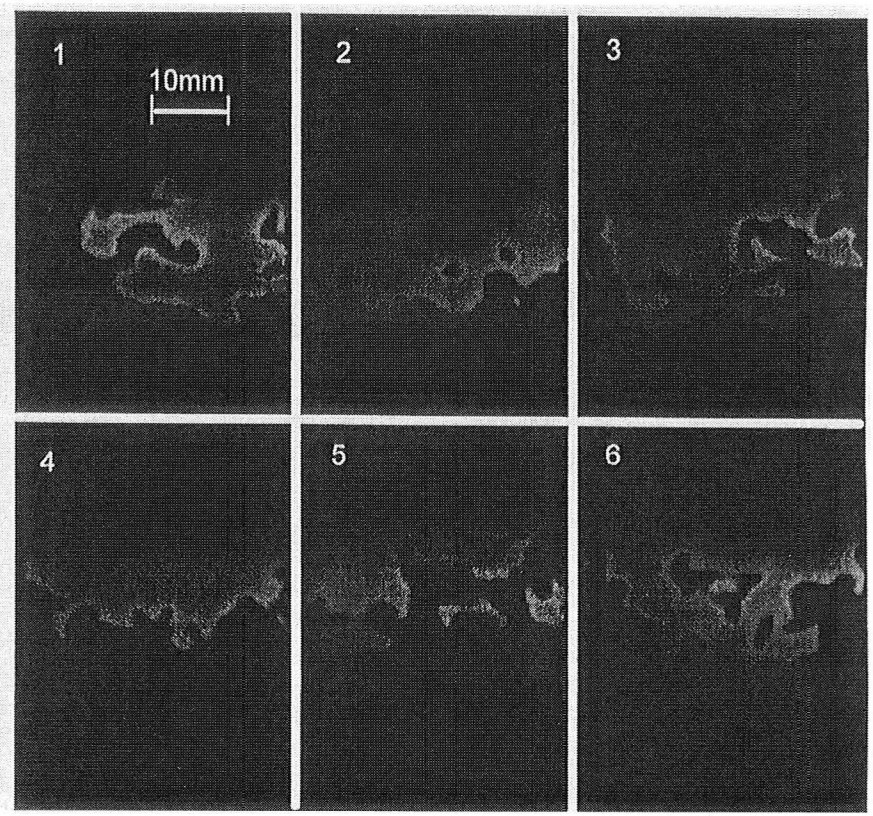

Figure 4(b) OH-PLIF images of Case IV

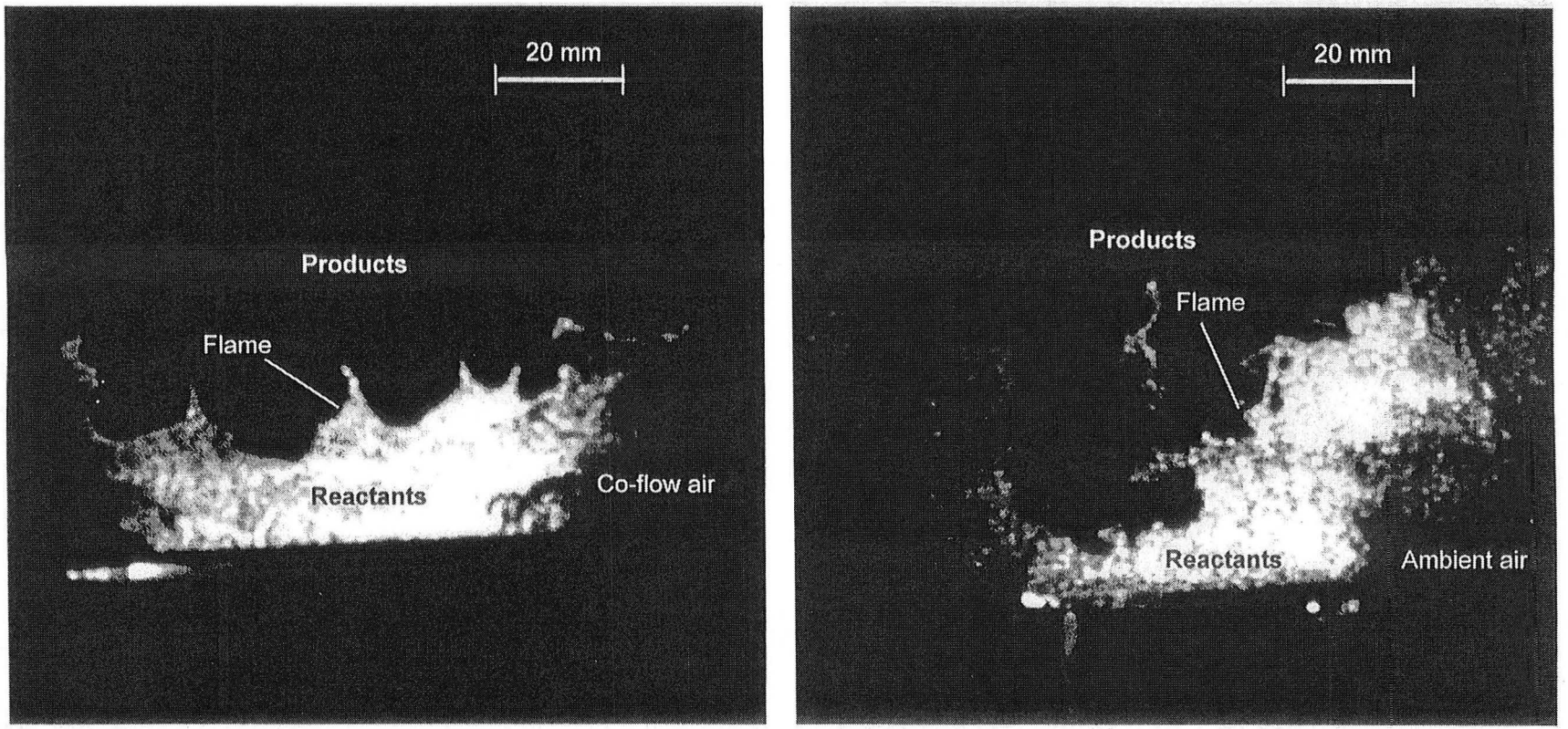

Figure 3 Tomographic records obtained for SWF12, a methane/air flame with moderate turbulence, and for Case IV.

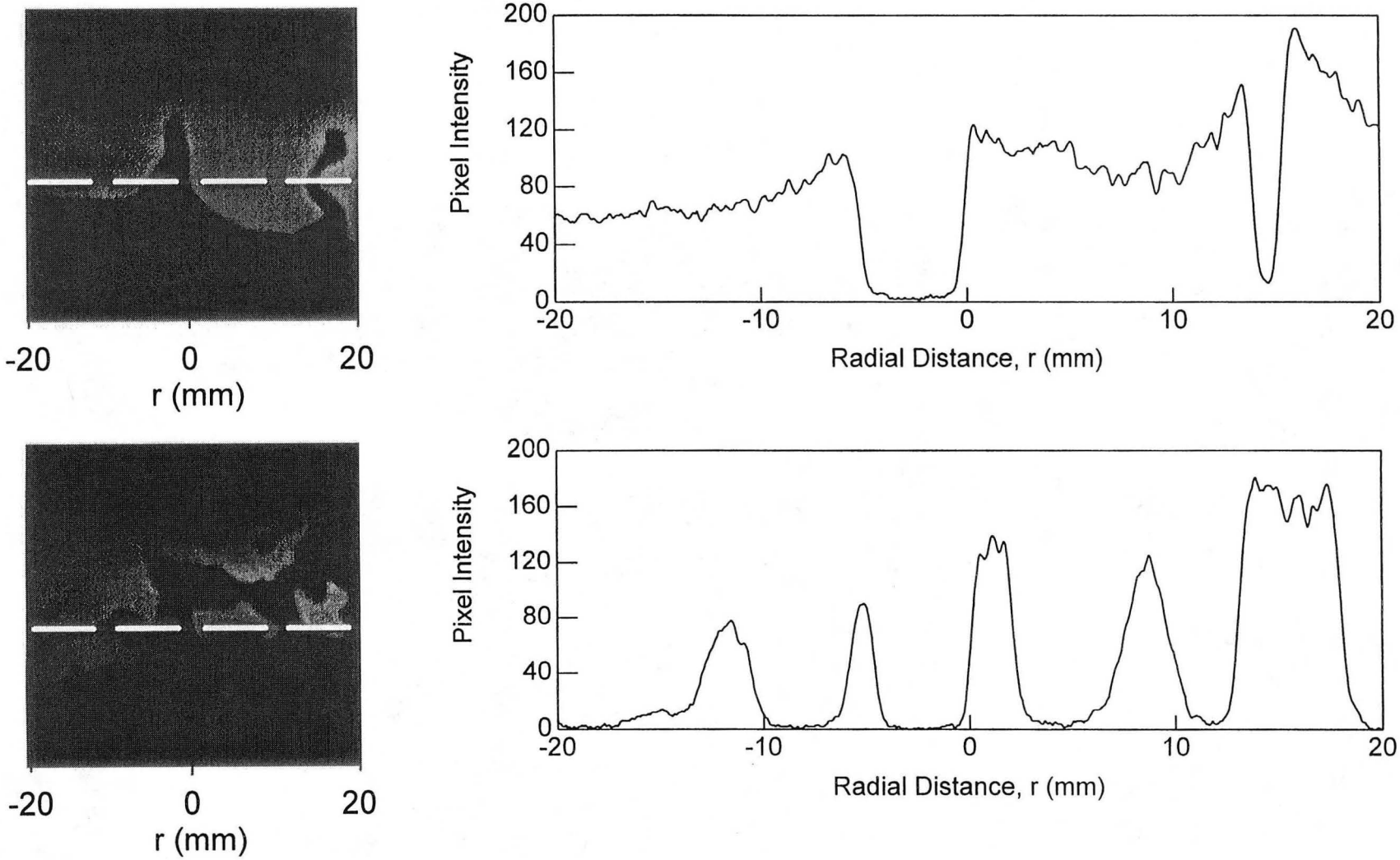

Figure 5 OH Intensity profiles extracted from two frames of Case II (top) and Case IV (bottom), the dashed lines on the PLIF images indicate the profile locations.

LAWRENCE BERKELEY NATIONAL LABORATORY
UNIVERSITY OF CALIFORNIA
TECHNICAL & ELECTRONIC INFORMATION DEPARTMENT
BERKELEY, CALIFORNIA 94720